Low-$\delta^{18}O$ mantle-derived magma in Panjal Traps overprinted by hydrothermal alteration and Himalayan UHP metamorphism: revealed by SIMS zircon analysis

Hafiz Ur Rehman [a]*

[a] Graduate School of Science and Engineering, Kagoshima University, Kagoshima 890-0065, Japan

Kouki Kitajima [b], John W. Valley [b]

[b] WiscSIMS Laboratory, Department of Geoscience, University of Wisconsin, 1215 W. Dayton St., Madison, WI 53706, USA

Sun-Lin Chung [c, d], Hao-Yang Lee [c, d]

[c] Department of Geosciences, National Taiwan University, Taipei, Taiwan

[d] Institute of Earth Sciences, Academia Sinica, Taipei, Taiwan

Hiroshi Yamamoto [a]

[a] Graduate School of Science and Engineering, Kagoshima University, Kagoshima 890-0065, Japan

Tahseenullah Khan [e]

[e] Department of Earth and Environmental Sciences, Bahria University, Islamabad, Pakistan

* Corresponding author

Hafiz Ur Rehman E-mail address: hafiz@sci.kagoshima-u.ac.jp

tel: +81-99-285-8147, fax: +81-99-259-4720

ABSTRACT

We report two generations of low-$\delta^{18}O$ zircons from the Himalayan eclogites and their host gneisses. In situ SIMS $\delta^{18}O$ analyses on single zircon crystals (with known age and Hf isotope ratios) from two populations of chemically distinct zircons demonstrate a complex history: (1) an early low-$\delta^{18}O$ mantle-derived magma, (2) followed by post-emplacement high-temperature meteoric-water alteration and finally (3) crystallization of new, low-$\delta^{18}O$ minerals during the ultrahigh-pressure metamorphism. Magmatic zircon (269 Ma) in Group I eclogites yielded $\delta^{18}O$ values from 1.9 to 4.6‰ VSMOW with an average value of 4.0 ± 0.2 (n = 35, the error is 2SD analytical precision and "n" represents number of analyzed spots), which is lower than the typical mantle values (5.3 ± 0.6, 2SD). In contrast, metamorphic zircons (45 Ma) in Group II eclogites preserve unusually low, negative $\delta^{18}O$ values from −3.9 to −2.7‰ (average: −3.4 ± 0.4, n = 35, 2SD). Zircons in felsic gneiss that surround Group II eclogites have inherited magmatic cores (ca. 260 Ma) with $\delta^{18}O$ values of ca. 2.9‰, which decrease to −0.1‰ in metamorphic (ca. 45 Ma) rims. These zircons preserve lower $\delta^{18}O$ values than would be equilibrated with typical mantle. The low-$\delta^{18}O$ values in magmatic zircons suggest that the mafic protolith to these eclogites formed from a hydrothermally altered subducted oceanic crust and the negative $\delta^{18}O$ values in metamorphic zircons indicate hydrothermal alteration after crystallization of the mafic

magmas but before growth of metamorphic zircons. This study reports evidence for melting of subducted low-$\delta^{18}O$ ocean crust to form low-$\delta^{18}O$ mantle-derived mafic magmas as previously proposed by Cartwright and Valley (1991, Geology 19, 578-581) for Proterozoic Scourie Dikes.

Keywords: Himalaya; Kaghan; Eclogites; Panjal Traps; In situ SIMS $\delta^{18}O$ analysis; zircon oxygen isotopes

1. INTRODUCTION

The $\delta^{18}O$ values (defined as $[(^{18}O/^{16}O_{sample} \div ^{18}O/^{16}O_{STD}) - 1] \times 1000$ in which the STD is Vienna Standard Mean Ocean Water; VSMOW) of mantle-derived magmas (basalts and gabbro) exhibit a narrow range of ca. +5.7 ± 0.3‰ (Eiler, 2001; Valley et al., 2005; Hoefs, 2015). The fairly homogenous $\delta^{18}O$ composition of a majority of mantle-derived rocks results because most of the mantle is well mixed in $\delta^{18}O$ and the oxygen isotope composition during magmatic fractionation remains almost the same. However, eclogite facies mantle nodules and silicate inclusions in diamond attest to mantle domains of subducted ocean crust with anomalous values of $\delta^{18}O$ that have been preserved (Garlick et al., 1971; Schulze et al., 2013). Higher $\delta^{18}O_{Wole\text{-}rock}$ values (> 6‰) are interpreted as upper oceanic crust that was altered by low temperature interaction with seawater and low $\delta^{18}O$ values (~0 to 5‰) are attributed to high temperature alteration of lower oceanic crust. Melting tends to homogenize these extreme values, but rare low-$\delta^{18}O$

mantle-derived magmas have been identified that are proposed to result from melting of subducted lower oceanic crust (Cartwright and Valley, 1991; 1992; Wei et al., 2002; Davies et al., 2015).

Low-$\delta^{18}O$ values can form subsolidus in metamorphic rocks through high temperature hydrothermal alteration by surface (marine or meteoric) water (Valley, 1986; Criss and Taylor, 1986; Zheng et al., 2003). Understanding the timing and source of low $\delta^{18}O$ values is crucial. However, it is difficult to determine the original magmatic source of metamorphic rocks with mixed protolith and complex evolutionary histories. Oxygen isotope ratios, combined with U–Pb age, and multi-isotope geochemistry, provide significant information regarding the nature of the source magma from which the rocks have crystallized and how they have been geodynamically evolved through time.

Zircon is a common accessory mineral in igneous, sedimentary, and metamorphic rocks, which provides a robust tool to unravel the history of Earth's crust and mantle. Zircons have been widely studied for U–Pb age dating, Hf isotopes, trace element geochemistry, and oxygen isotope ratios. Because of its chemical and physical inertness and resistance to alteration, crystalline zircon (i.e., not radiation damaged) can retain compositions from crystallization (Wasserburg et al., 1969; Compston et al., 1984; Gebauer, 1996; Liati and Gebauer, 1999; Belousova et al., 2010; Valley, 2003; Valley et al., 2005, 2015; Liu et al., 2006). Moreover, due to the extremely slow diffusion rate of oxygen in zircon (Watson and Cherniak, 1997; Zheng and Fu, 1998; Peck et al., 2003; Page et al., 2007; Bowman et al., 2011) it can preserve the original $\delta^{18}O$ values of the source from which it crystallized. Thus, zircons can provide the key for understanding the evolutionary history of rocks. If zircons are zoned or have

chemically distinct domains (Chen et al., 2011), then combined in situ U–Pb age, Hf isotope, and $\delta^{18}O$ data in zircon provide critical information to trace back the geodynamic evolution from magmatic to post-magmatic, and subsequent metamorphic events.

In this study we report very low and negative $\delta^{18}O$ values of magmatic and metamorphic zircons (with known U–Pb age and Hf isotope compositions; Rehman et al., 2013a, 2016) from Himalayan eclogites and their host gneisses. The aim of this study is to determine the composition of pre-eclogite magmas from which these rocks formed and how they hydrothermally altered. Finally, what happened to their chemistry when these rocks were subjected to ultrahigh-pressure metamorphism at mantle depths (coesite-stability) and subsequent exhumation. These results yield significant insight into the evolution of the Indian plate before and after its breakup from Gondwana and the Eocene India-Asia collision.

2. SAMPLE DESCRIPTION AND GEOLOGICAL BACKGROUND

In this study six 25-mm diameter zircon mounts were analyzed: two mounts from one sample of high-pressure (HP) Group I eclogite (Ph380_Zrn2 and Ph380_Zrn3); two mounts containing zircons from three samples (Ph422, Ph423, and Ph425) of ultrahigh-pressure (UHP) Group II eclogites ("A" and "B"); and two mounts of zircons from two UHP felsic gneisses that surround the Group II eclogites (Ph416 and Ph427). Petrological details of Groups I and II eclogites and felsic gneisses were discussed

115 elsewhere (Rehman et al., 2014, 2016, 2017). A brief description of the samples used in
116 this study is presented below.

117 Both groups of eclogite and felsic gneiss were collected from the Higher
118 Himalayan crystalline sequence in the Kaghan Valley, Pakistan (Fig. 1). Group I
119 eclogites are medium to coarse-grained, composed of garnet porphyroblasts, omphacite,
120 amphibole, and symplectites replacing garnet and omphacite with abundant rutile,
121 titanite, and ilmenite. Zircons are abundant and relatively large (~500 μm). Pressure-
122 temperature conditions of 2.2 ± 0.3 GPa and 704 ± 92 ºC were previously reported from
123 this group (Rehman et al., 2013b). Group II eclogites are composed of garnet,
124 omphacite, phengite, epidote, and quartz/coesite, with accessory rutile, titanite and a
125 few small zircons (<200 μm). Group II eclogites recorded conditions around 2.7–3.2
126 GPa and 727–786ºC confirming their UHP stability (O'Brien et al., 2001; Kaneko et al.,
127 2003; Rehman et al., 2007). Felsic gneisses are composed of quartz, white mica, biotite,
128 plagioclase and epidote with accessory rutile, titanite, apatite, allanite and zircon. Felsic
129 gneisses do not preserve UHP phases in the matrix or as inclusions in major
130 porphyroblasts however coesite inclusions in zircons from felsic gneiss (Rehman et al.,
131 2016) confirm their UHP history. The protolith of both types of eclogite (as well as
132 other low-grade metabasites) were proposed to be derived from large-scale magmatic
133 activity (known as the Panjal Traps) on the Indian plate in the Permian (for details see
134 Rehman et al., 2016, and references therein). The relatively coarser grained Group I
135 eclogites were probably derived from gabbroic protolith whereas the finer-grained
136 Group II eclogites, preserving UHP phase, most likely developed from basaltic protolith.
137 Mafic lithologies, older than Permian, are rare or have not been reported from the

western Himalaya. However, granitic rocks of Cambro-Ordovician age (ca. 460 to 490 Ma) and associated mafic and felsic volcanics have been identified along the entire Himalayan range indicating an extensive regional orogenic event in the northern Indian continent (e.g. Mansehra granite in Pakistan, Mandi granite in India, Bhimphedian granite in Nepal, and bimodal volcanism in southwest Yunnan and Tibet in China) which were interpreted to represent the northern margin of east Gondwana (Miller et al., 2001; Cawood et al., 2007; Zhu et al., 2012; Naeem et al., 2016).

3. ANALYTICAL TECHNIQUES

Most of the zircons of this study were previously analyzed for U–Pb and Hf isotopes (see Rehman et al., 2016). In this study, in situ analysis of oxygen isotope ratios ($^{18}O/^{16}O$) was performed on zircon grains using a CAMECA IMS 1280 ion microprobe at the WiscSIMS Laboratory of the University of Wisconsin-Madison, following established procedures (Kita et al., 2009; Valley and Kita, 2009; Kitajima et al., 2012). Oxygen isotopes were analyzed using a 2.0 – 2.2 nA primary $^{133}Cs^{+}$ beam with ~10 μm spot size. Secondary ^{16}O and ^{18}O ions were measured simultaneously using two Faraday cup detectors. As a monitor of "water" and radiation damage, $^{16}O^{1}H$ was analysed simultaneously with ^{18}O and ^{16}O and from the same pit (Wang et al., 2014). On all six 25-mm diameter mounts, chips of KIM-5 zircon (WiscSIMS standard with $\delta^{18}O$ = 5.09‰ VSMOW, Valley, 2003) were mounted at the center and sample zircon grains were within 7 mm of the center. All the mounts were re-polished to keep the standard

and other grains at equal height. Topography of the sample surface was checked by profilometer before analysis to ensure all the grains are at the same height as surrounding epoxy. Zircon mounts were ultrasonically cleaned with deionized water and alcohol, and gold coated prior the SIMS analysis. Oxygen isotope data were acquired for all the six mounts in a single 12-hour session. The average value of eight standard analyses bracketing each group of 10 to 14 analyses of unknowns was used for instrumental mass bias correction. The precision of individual analyses is estimated by two standard deviations (2SD) of the reproducibility of bracketing standard analyses and measured values for this session average < 0.3‰ (Valley and Kita, 2009). The results of $^{18}O/^{16}O$ ratios are reported in per mil "‰" notation relative to the Vienna Standard Mean Ocean Water (VSMOW).

4. RESULTS

A total of 97 spots (two to three spots on each of 43 zircon grains) on six mounts were measured for $\delta^{18}O$. Measured spots on Groups I and II eclogite, and felsic gneisses are shown in Figs. 2, 3, 4, respectively. Near the measured spots, we also show U–Pb age and εHf(t) values for previously analyzed grains (from Rehman et al., 2016). Data for the analyzed zircons are shown in table 1, and the data with all details for the analyzed zircons and standards are provided in supplementary table S1 (available on line). Values of $\delta^{18}O$ range from 1.9 to 4.6‰ (average = 4.0 ± 0.2 standard's internal error here and elsewhere when stated, n=35 in which notation "n" means number of analyzed spots) in zircons of Group I eclogites, from −3.8 to −2.7‰ (average: −3.4 ± 0.4, n=35) in zircons

of Group II eclogites, and from −0.1 to 2.9‰ (average: 1.1 ± 0.1, n=27) in zircons of felsic gneiss. The $\delta^{18}O$ values of zircons in Group I eclogites are relatively variable but within a limited range. These values could be attributed to the earlier events and have been potentially acquired from the magmatic source. In contrast, $\delta^{18}O$ values of zircons in Group II eclogites display a narrow range from a more homogenised protolith (Fig. 5). The $\delta^{18}O$ values in two distinct populations of zircons are in accord with the U–Pb age data from the analyzed grains in which the former group yielded ages related to the magmatic events and the later produced ages representing the Himalayan UHP eclogite facies event. There was no distinction for core vs. rim domains in Group I zircons and most of the dated spots show protolith-related ages (Fig. 2, also see Rehman et al., 2016). Several spots show younger ages than the geologically known events for the eclogite protolith; however they show no significant difference in $\delta^{18}O$ values. In contrast, all of the zircon grains in Group II eclogites are metamorphic in origin (containing inclusions of garnet, omphacite, and rutile) representing growth/recrystallization during the Himalayan UHP event (Fig. 3) and we could distinguish core and rim domains in zircons from the felsic gneisses (seen via SEM-CL images) in which the core yielded ages identical or slightly younger than those obtained from the zircons of Group I eclogites and the rim yielded metamorphic ages coeval to those of zircons in Group II eclogites (Fig. 4). It is worthy of note that all the grains from both types of eclogite and from the surrounding felsic gneisses preserve $\delta^{18}O$ values lower than the typical mantle-equilibrated range (Fig. 6), however Group II eclogites show anomalously low, negative $\delta^{18}O$ values. Zircons in felsic gneisses also

exhibit lower $\delta^{18}O$ values and core domains preserve relatively higher $\delta^{18}O$ values compared with the rim or outer domains (Fig. 5).

5. DISCUSSION

The $\delta^{18}O$ values in zircons (Group I, II, and felsic gneisses) exhibit a narrow range within each group and are significantly lower than those equilibrated with the mantle. Whole-rock and other constituent minerals from the three rock types also show lower than the typical mantle equilibrated values (zircon and whole rock data are shown in Fig. 7; other data are presented in supplementary table S2, reproduced from Rehman et al., 2014). These features suggest that one or more of the following scenarios account for the unusually low $\delta^{18}O$ values in the studied samples. First, hydrothermal alteration of the source of Panjal magmas occurred, prior to subduction, followed by low-$\delta^{18}O$ fluid (meteoric water) interaction at high temperature with the protolith of eclogites, then low $\delta^{18}O$ metamorphic minerals were formed during high-temperature metamorphism from their precursors. In the forthcoming sections we discuss these scenarios in detail. The narrow range of $\delta^{18}O$, U–Pb age concordance and low OH/O ratios indicate that the studied zircons preserve primary mineral compositions and thus rule out a forth possibility; the analyzed $\delta^{18}O_{zircon}$ values were not affected by secondary alteration or radiation damage.

Crystalline, non-metamict zircon, due to its resistance to hydrothermal alteration (Valley et al., 1994, 2005; Watson and Cherniak, 1997; Zheng and Fu, 1998; Wei et al.,

227 2002; Zheng et al., 2004), preserves $\delta^{18}O$ of the magma from which it crystallized.
228 However, under higher temperatures (> 800 to 900°C) the values of $\delta^{18}O$ in crystalline
229 zircon may partially reset due to diffusion (e.g. Valley, 2003; Page et al., 2007;
230 Bowman et al., 2011). In contrast, zircons with high levels of radiation damage,
231 domains within zircon become amorphous (metamict) and are easily altered. There are
232 many tests that, in combination, permit identification of such non-crystalline material,
233 including: discordance of U–Pb ages, CL zoning patterns, magnetism, solubility in HF,
234 trace element compositions, low birefringence, microcracks and OH/O ratios (Valley,
235 2003; Wang et al., 2014; Valley et al., 2005, 2015). We carefully investigated the
236 analyzed zircons in this study to determine if they incorporate any significantly
237 damaged domains or metamictization. Most of the analyzed spots in zircons of Group I
238 eclogite yielded U–Pb ages (ca. 259 ± 10 Ma) that plot on Concordia.

239 The positive εHf(t) values cluster around +10 (ranging between +4.2 and +14.5)
240 represent a juvenile mantle source with almost no crustal component (see Rehman et al.,
241 2016 for details on Hf isotope discussion). Zircons in Group II eclogite are more
242 homogeneous in geochemical features showing U–Pb ages within a narrow range (41 to
243 53 Ma, average: 48 ± 3, 1SD) also plot on Concordia. The εHf(t) values in this group
244 cluster around +7 (ranging between +3.4 to +8.9) and represent a common juvenile
245 mantle source similar to that of Group I zircons. These features suggest that Group I
246 zircons represent magmatic crystallization at ~269 Ma while Group II formed from the
247 crystallization of new zircons during metamorphism of hydrothermally altered low-$\delta^{18}O$
248 rocks (Fig. 7). We also took care not to analyze areas close to the healed cracks or
249 above visible micro inclusions. Our data show extremely low background-corrected

250 $^{16}O^{1}H/^{16}O$ ratios (supplementary table S1) and there is no correlation of $^{16}O^{1}H/^{16}O$
251 versus $\delta^{18}O$ (Fig. 8). This evidence further attests that no secondary alteration was
252 experienced by those zircons; hence the oxygen isotope data reported here are unaltered
253 and geologically meaningful.

254 Moreover, solid-state diffusive exchange of oxygen can be observed with
255 obvious steep gradients under the extreme temperature conditions (e.g. ultrahigh-
256 temperature metamorphism >800 °C: Page et al., 2007; Bowman et al., 2011). The
257 studied samples have experienced HP to UHP eclogite facies metamorphism
258 (750~800 °C). Diffusive exchange, even if it occurred, should be relatively slower at
259 such conditions. Therefore, the protolith-related U–Pb age in magmatic zircons in
260 Group I eclogite as well as the core domains of zircons in felsic gneisses most likely
261 preserve the parent magma $\delta^{18}O$ values whereas the newly grown metamorphic zircons
262 in Group II eclogite have likely acquired unusually low $\delta^{18}O$ values from metamorphic
263 growth in lower $\delta^{18}O$ rocks. In contrast, Group II zircons and rim domains in zircons
264 from felsic gneisses likely grew under UHP conditions at 750~800 °C and hence record
265 metamorphic equilibration of isotope ratios and trace element compositions. The
266 negative $\delta^{18}O$ values of zircons in Group II eclogites record the composition of the
267 whole rock prior to metamorphism. That is why $\delta^{18}O$ values in garnet and omphacite
268 are nearly identical to those of zircons. However, magmatic zircons in Group I eclogites
269 retain $\delta^{18}O$ values from their parent magma. During later exhumation stages, the
270 $\delta^{18}O_{zircon}$ values were unchanged because of the relatively slower diffusion rate of
271 oxygen in crystalline zircon.

The $\delta^{18}O$ values in UHP felsic gneisses are also low compared to normal granitic, volcanic or metasedimentary rocks (Fig. 6). Zircons in felsic gneisses retain low but slightly positive $\delta^{18}O$ values in core domains, but have negative values in rim domains. These features indicate two episodes of high temperature hydrothermal alteration. The protolith of felsic magmas was altered by low-$\delta^{18}O$ water before melting and the igneous rocks exchanged with heated meteoric water after solidification, which further reduced $\delta^{18}O$ to negative values. Finally, the hydrothermally altered, low-$\delta^{18}O$ protoliths were transformed into eclogites and gneisses when these rocks reached mantle depths (> 90 km; coesite stability) in the Eocene during the India-Asia collision. Values of $\delta^{18}O$ equilibrated among the metamorphic mineral assemblages under the HP/UHP conditions. During late exhumation, fluids from the surrounding metasedimentary rocks (carbonates/pelites) potentially once again modified $\delta^{18}O$ values of some minerals to be equal or higher than the typical mantle range, as can be seen in the amphibolites ($\delta^{18}O_{whole\text{-}rock}$ ~5.8‰) and greenschist ($\delta^{18}O_{whole\text{-}rock}$ ~9.2‰, supplementary table S2, reproduced from Rehman et al., 2014).

A correlation of $\delta^{18}O$ between quartz and zircon, if seen with appropriate fractionation ($\Delta^{18}O_{quartz\text{-}zircon}$ ~2‰ at magmatic temperatures, Valley et al. 2003), would suggest that both minerals were isotopically equilibrated at higher temperatures when zircon crystallized. However, in the $\delta^{18}O_{quartz}$ versus $\delta^{18}O_{zircon}$ plot (Fig. 9), the $\delta^{18}O_{quartz\text{-}zircon}$ data from Group I plot away from the quartz-zircon ($\Delta^{18}O_{quartz\text{-}zircon}$ = 2‰) equilibration line (please note that the data plotted represent an average value of all the analyzed spots). These features indicate that metamorphism or any other secondary events did not modify the zircon oxygen isotope data from the time of its magmatic

crystallization. To further confirm that the $\delta^{18}O_{zircon}$ is primary, we plot $\delta^{18}O_{garnet}$ versus $\delta^{18}O_{zircon}$ in the same figure (Fig. 9) in which garnet-zircon data in Group I also plot away from the garnet-zircon equilibration line ($\Delta^{18}O_{garnet\text{-}zircon}$ = 0‰). This evidence supports our interpretation that $\delta^{18}O_{zircon}$ is primary and did not equilibrate with $\delta^{18}O_{garnet}$. For the Group II where all zircons are metamorphic, the $\Delta^{18}O_{quartz\text{-}zircon}$ data plot further away from the quartz-zircon equilibration line, indicating that the $\delta^{18}O$ values of zircon and quartz were not in equilibrium during metamorphism. In contrast, $\delta^{18}O_{garnet}$ versus $\delta^{18}O_{zircon}$ in Group II plot along and parallel to the garnet-zircon equilibration line, indicating that garnet and metamorphic zircons in Group II eclogites acquired lower, nearly identical $\delta^{18}O$ values when they were in equilibrium during eclogite facies metamorphism ($\Delta_{garnet\text{-}zircon}$ ~0.1‰ for almandine-pyrope at metamorphic temperatures, Valley, 2003). These metamorphic minerals acquired the low-$\delta^{18}O$ values from the metamorphic protolith. In contrast, zircons in Group I eclogites preserve higher $\delta^{18}O$ values than those found in garnet in the same group, indicating lack of equilibration among igneous zircons and eclogite facies minerals.

5.1. LOW-$\delta^{18}O$ MAFIC MAGMA

Rehman et al. (2014) discussed the possibility of a low-$\delta^{18}O$ magma reservoir for the Permian Panjal Traps based on bulk analysis of $\delta^{18}O$ in whole-rock powders and minerals. In this study, based on the new in situ $\delta^{18}O$ data from magmatic and metamorphic zircons from the same rocks, we present further insights for magma genesis and post-magmatic evolution.

There are numerous examples of low-$\delta^{18}O$ magmas that formed in the crust, including: Icelandic basalts (Hartley et al., 2013), felsic volcanics from Yellowstone and other centers of the Snake River Plain (Bindeman and Valley, 2001; Bindeman et al., 2008; Blum et al., 2016), UHP eclogites and granitic gneisses from the Dabie-Sulu orogenic belt in eastern China (Zheng et al., 1998; Rumble et al., 2002; Wei et al., 2008; Fu et al., 2013; Wan et al., 2013; He et al., 2016) and mafic dykes of the Anorogenic Koegel Fontein Complex, South Africa (Curtis et al., 2013). Low $\delta^{18}O$ values in Icelandic basalts were due to the magmatic assimilation of altered low- $\delta^{18}O$ wallrocks during its ascent through the crust (Hartley et al., 2013). In mafic dykes of the Koegel Fontein Complex, the lower $\delta^{18}O$ values (ca. −2‰) were attributed to the partial melting of hydrothermally altered low-$\delta^{18}O$ country rocks forming low $\delta^{18}O$-depleted crustal magmas (Curtis et al., 2013).

Partial melting of hydrothermally altered volcanics was proposed by several authors for the genesis of low $\delta^{18}O$ rhyolites of the Snake River Plain (e.g. Bindeman and Valley, 2001; Blum et al. 2016). For eastern China eclogites, the low or negative $\delta^{18}O$ values were acquired by melting or assimilation of low-$\delta^{18}O$ crustal rocks (e.g. Yui et al., 1995; Wang et al., 2011; Fu et al., 2013; He et al., 2016 and references therein). Additionally, low $\delta^{18}O$ granite in northeast China was formed by the partial melting of hydrothermally altered crustal material which exchanged with low-$\delta^{18}O$ surface fluids at high temperature during the continental rift tectonics associated with the breakup of Rodinia supercontinent (Wei et al., 2002; Zheng et al., 2007, 2008; He et al., 2016).

In contrast to crustal magmas, low-$\delta^{18}O$ magmas that formed in the mantle are rare. Low $\delta^{18}O$ tholeiitic magmas intruded the Lewisian Complex to form Scourie dikes in the Paleoproterozoic (Cartwright and Valley, 1991, 1992; Davies et al., 2015). These magmas are interpreted to be uncontaminated and represent primitive mantle melts formed from melting of subducted oceanic crust that was hydrothermally altered before subduction (Cartwright and Valley, 1991). The low $\delta^{18}O$ values of zircons in Group I eclogites (average = 4.0‰) suggest melting of a low-$\delta^{18}O$ source. As the values of $\delta^{18}O$ in zircon of Group I eclogites are lower (1.9 to 4.6‰) than the mantle values (4.7 to 5.9‰) they reflect a source that was hydrothermally altered by surface waters (seawater or meteoric water) prior to magma generation. The negative $\delta^{18}O$ in Group II zircons (−3.9 to −2.7‰) and those in the whole rock cannot be formed without the meteoric water-rock interaction. To explain the process of seawater-hydrothermal alteration of the source, we have to look back at the tectonic scenario of the Indian plate-Tethyan-Asian subduction and collision. A significant component of the Tethyan oceanic crust, north of the MMT (suture between Indian plate and Kohistan-Ladakh Arc), has been subducted before the India-Asia collision. However there is no coherent oceanic crustal mass within the Himalayan metamorphic belt (except the Panjal mafic volcanics) south of MMT. In fact, crust forming events in Cambro-Ordovician time (ca. 460 to 490 Ma) along the northern margin of Indian continent during an Andean-type proto-Tethyan subduction (e.g. Miller et al., 2001; Cawood et al., 2007; Zhu et al., 2012; Naeem et al., 2016) may have played a significant role to underplate the oceanic crust and possibly contributed to the parent magma of the Permian Panjal Traps. Our hypothesis is consistent with the model of Cawood et al. (2007, see their Fig. 5) who proposed that mafic underplating, terrane accretion, and crustal thickening occurred in the Cambro-

362 Ordovician. We speculate that part of the hydrothermally altered subducted oceanic
363 crust could have melted and formed the protolith of Himalayan eclogites during the
364 Permian Panjal Trap extensive magmatism (continental flood basalts and feeder dikes).

365 Hafnium isotope data provide further insights on the origin of magmatic source.
366 The Hf isotope data from the analyzed zircons in Groups I and II eclogites, and felsic
367 gneiss show an average depleted mantle (T_{DM}) model age of 487 Ma (ranging from 307
368 to 709 Ma, n = 20) for Group I zircons, 455 Ma (ranging from 242 to 569 Ma, n = 38)
369 for Group II zircons, and 440 Ma (ranging from 300 to 573 Ma, n = 22) for zircons in
370 felsic gneiss (see Table 3 in Rehman et al., 2016). The Hf model age does not represent
371 the age of zircon crystallization but is the time at which the Hf of a crustal rock was
372 isolated from its depleted mantle source. The Hf average T_{DM} model age from the
373 studied zircons fits well with the magmatic source of Cambro-Ordovician orogenic
374 events reported along the eastern margin of Gondwana. The 460 to 490 Ma Mansehra
375 granite, located south of the Kaghan Valley (Naeem et al., 2016), the 496 ± 14 Ma
376 tholeiitic mafic rocks of Mandi pluton in India (Miller et al., 2001), the 475 Ma
377 Bhimphedi granites in Nepal (Cawood et al., 2007), and the bimodal volcanism in Tibet
378 (Zhu et al., 2012) indicate asthenospheric upwelling and crustal extension tectonics
379 during the Cambro-Ordovician time. All the zircons analyzed in this study yield positive
380 $\varepsilon_{Hf}(t)$ values indicating their source was segregated from a short-lived juvenile mantle
381 crust. We suspect the low-$\delta^{18}O$ values in magmatic zircons (Group I) were acquired
382 from the remelting of the hydrothermally altered subducted oceanic crust.

383 In contrast to values of $\delta^{18}O_{zircon}$ that are low, but positive, alteration by low-
384 $\delta^{18}O$ meteoric water is necessary to form negative $\delta^{18}O$ values as preserved in the

zircons of Group II eclogites, felsic gneisses, and those preserved in whole rock samples. This would require at least minimum initial water $\delta^{18}O$ values < −8‰ or even lower to produce negative $\delta^{18}O$-bearing rocks. After the Panjal Trap magmatism the mafic and associated lithologies (including sedimentary successions) could have been severely altered by low-$\delta^{18}O$ meteoric water, which lowered $\delta^{18}O$ values of the exchangeable minerals in the whole-rock, but did not exchange with refractory minerals like zircon (supplementary table S2, available on line). Values of $\delta^{18}O$ in Group II eclogites (whole rock and most of the constituent minerals, excluding late-stage phases) are much lower than in Group I (Rehman et al., 2014). Rocks with such negative $\delta^{18}O$ values cannot be produced without meteoric water interaction at high temperatures. None of the ages analyzed in zircons from Group II eclogites are reasonable magmatic ages for the protolith. The evidence clearly demonstrates that the metamorphic domains (ca. 45 Ma) acquired $\delta^{18}O$ values from their pre-metamorphic precursors. The rim domains of zircons in felsic gneisses (ca. 45 Ma) also preserve low-$\delta^{18}O$ values and further support our interpretation that the post-magmatic protoliths of both types of rocks (mafic and felsic) were hydrothermally altered by meteoric water before subduction-related metamorphism.

5.2. POST-MAGMATIC METEORIC WATER-ROCK INTERACTION

As discussed earlier, seawater-rock interaction ($\delta^{18}O_{sea\ water}$ = 0‰) will not form negative $\delta^{18}O$ values in rocks even at high temperature (>300°C). Likewise, meteoric

407 water of −4‰ at low near-surface temperatures (< 100°C) cannot alter basaltic rocks
408 (5.7‰) to negative $\delta^{18}O$ values even if the water-rock interaction ratios are high (see
409 Zhao and Zheng, 2003). Altering mantle-composition rocks to values of $\delta^{18}O$ below
410 −3‰ will require involvement of meteoric water. These lines of evidence show that
411 heated meteoric water-rock interaction likely altered the Panjal basaltic rocks after
412 crystallization and these low or negative $\delta^{18}O_{whole\text{-}rock}$ values were preserved despite
413 UHP metamorphism during the India-Asia collision-related subduction. The $\delta^{18}O$ of
414 zircons in both groups of low-$\delta^{18}O$ eclogite confirm seawater hydrothermal alteration of
415 the pre-magmatic source, followed by post-magmatic meteoric water hydrothermal
416 alteration. Magmatic core domains of zircons in felsic gneisses (with U–Pb ages of 260
417 Ma) show a trend of decrease in $\delta^{18}O_{zircon}$ values ca. 2.9 to −0.1‰ from the magmatic
418 cores towards metamorphic rims. Prolonged meteoric water-rock interaction can be
419 traced from the negative $\delta^{18}O_{whole\text{-}rock}$ values, but zircons, once crystallized (e.g., Group
420 I), will faithfully preserve the $\delta^{18}O$ value from its parent magma. Thus, metamorphic
421 zircons in Group II eclogites and rim domains of zircons in felsic gneisses acquired
422 low-$\delta^{18}O$ values from later conditions when they grew. This interpretation is supported
423 by $\delta^{18}O_{whole\text{-}rock}$ values that are significantly lower than $\delta^{18}O_{zircon}$ in Group I eclogites
424 indicating post-magmatic high-temperature hydrothermal alteration; the negative $\delta^{18}O$
425 values in the pre-metamorphic protolith were reequilibrated during eclogite facies
426 metamorphism. Our results are consistent and comparable with the hydrothermal
427 meteoric water alteration to the UHP eclogites and granitic gneisses in the Dabie-Sulu
428 orogenic belt.

429

6. CONCLUSIONS

The Permian-age Group I eclogites formed from equivalents of the Panjal Traps and contain low-$\delta^{18}O$ igneous zircons preserved from unusual, low-$\delta^{18}O$ mantle-derived magmas with hydrothermally altered subducted protoliths. The core domains of zircons in felsic gneisses also have lower $\delta^{18}O$ than the normal mantle-equilibrated value. After crystallization, these rocks were hydrothermally altered by heated meteoric water shifting $\delta^{18}O$ to negative values. Finally, during subduction of the Indian plate under Asia in the Eocene, $\delta^{18}O$ values in newly formed zircons were reequilibrated during UHP metamorphism in Group II eclogites and rim domains of zircons in felsic gneisses.

ACKNOWLEDGEMENTS

We thank Noriko Kita and Jim Kern of the WiscSIMS Lab for help during SIMS analysis of $\delta^{18}O$. We also thank Emily Hung for help in zircon U–Pb age and Hf isotope analyses. This work was supported by the JSPS Research Fund (Kakenhi # 15K05316 and partly by the MOST project # 1050021585). The WiscSIMS Lab is supported by NSF (EAR-1355590) and the University of Wisconsin- Madison.

REFERENCES

Alt, J.C., Muehlenbachs, K., Honnorez, J., 1986. An oxygen isotopic profile through the upper kilometer of the oceanic crust, DSDP Hole 504B. Earth and Planetary Science Letters **80**, 217-229.

452 Baumgartner, L.P., Valley, J.W., 2001. Stable Isotope Transport and contact
453 Metamorphic Fluid Flow: In: Valley JW and Cole DR (eds) Stable Isotope
454 Geochemistry, Reviews In Mineralogy and Geochemistry, **43**, 415-468.
455 Belousova, E.A., Kostitsyn, Y.A., Griffin, W.L., Begg, G.C., O'Reilly, S.Y., Pearson,
456 N.J., 2010. The growth of the continental crust: Constraints from zircon Hf-
457 isotope data. Lithos **119**, 457-466.
458 Bindeman, I.N., Valley J.W., 2001. Low-$\delta^{18}O$ rhyolites from Yellowstone: magmatic
459 evolution based on analyses of zircons and individual phenocrysts. Journal of
460 Petrology **42**, 1491-1517.
461 Bindeman, I.N., Fu B., Kita, N., Valley, J.W., 2008. Origin and evolution of silicic
462 magmatism at Yellowstone based on ion microprobe analysis of isotopically zoned
463 zircons. Journal of Petrology **49**, 163-193.
464 Blum, T.B., Kitajima, K., Nakashima, D., Spicuzza, M.J., Strickland, A., Valley, J.W.,
465 2016. Low-$\delta^{18}O$ magmas of the Lake Owyhee volcanic field, Oregon: Implications
466 for low-$\delta^{18}O$ magmas of the Snake River Plain - Yellowstone hotspot and other
467 low-$\delta^{18}O$ large igneous provinces, Contributions to Mineralogy and Petrology **171**:
468 92, DOI.org 10.1007/s00410-016-1297-x.
469 Bowman, J.R., Moser, D.E., Valley, J.W., Wooden, J.L., Kita, N.T., Mazdab, F.K., 2011.
470 Zircon U–Pb isotope $\delta^{18}O$ and trace element response to 80 m.y. of high
471 temperature metamorphism in the lower crust: Sluggish diffusion and new records
472 of Archean craton formation. American Journal of Science **311**, 719-772.
473 Cartwright, I., Valley, J.W., 1991. Low-^{18}O Scourie dike magmas from the Lewisian
474 Complex, northwestern Scotland. Geology **19**, 578-581.

475 Cartwright, I., Valley, J.W., 1992. Oxygen isotope geochemistry of the Scourian
476 Complex, NW Scotland. Journal of the Geological Society, London **149**, 115-126.
477 Cawood, P. A., Johnson, M. R. W., Nemchin, A. A., 2007. Early Palaeozoic orogenesis
478 along the Indian margin of Gondwana: Tectonic response to Gondwana assembly.
479 Earth and Planetary Science Letters **255**, 70-84.
480 Chen, Y. X., Zheng, Y. F., Chen, R. X., Zhang, S. B., Li, Q., Dai, M., Chen, L., 2011.
481 Metamorphic growth and recrystallization of zircons in extremely 18O-depleted
482 rocks during eclogite-facies metamorphism: Evidence from U-Pb ages, trace
483 elements, and O-Hf isotopes. Geochimica et Cosmochimica Acta **75**, 4877-4898.
484 Cherniak D.J., Watson, E.B., 2000. Pb diffusion in zircon. Chemical Geology **172**, 5-24.
485 Compston, W., Williams, I.S., Meyer, C., 1984. U–Pb geochronology of zircons from
486 lunar breccia 73217 using a sensitive high mass-resolution ion microprobe.
487 Journal of Geophysical Research **89B**, 525-534.
488 Criss, R.E. and Taylor, H.P., 1986. Meteoric-Hydrothermal systems. in: Valley, J.W.,
489 Taylor, H.P. Jr., O'Neil, J.R. (Eds.), Stable Isotopes in High Temperature
490 Geological Processes, Reviews in Mineralogy **16**, 373-424.
491 Curtis, C.G., Harris, C., Trumbull, R.B., Beer, C., Mudzanani, L., 2013. Oxygen isotope
492 diversity in the anorogenic Koegel Fontein Complex of South Africa: a case for
493 basement control and selective melting for the production of low $\delta^{18}O$ magmas.
494 Journal of Petrology **54**, 1259-1283.
495 Davies, J.H.F.L., Stern, R.A., Heaman, L.M., Rojas, X., Walton, E.L. 2015. Resolving
496 oxygen isotope disturbance in zircon: A case study from the low $\delta^{18}O$ Scourie
497 dikes, NW Scotland. American Mineralogist **100**, 1952-1966.

Fu, B., Kita, N., Wilde, S.A., Liu, X., Cliff, J., Greig, A., 2013. Origin of the Tongbai-Dabie-Sulu Neoproterozoic low-$\delta^{18}O$ igneous province, east-central China. Contributions in Mineralogy and Petrology **165**, 641-662.

Garlick, G.D., MacGregor, I.D., Vogel, D.E., 1971. Oxygen isotope ratios in eclogites from kimberlites. Science **172**, 1025-1027.

Gebauer, D., 1996. A P–T–t-path for an (ultra?-) high-pressure ultramafic/mafic rock-association and its felsic country-rocks based on SHRIMP-dating of magmatic and metamorphic zircon domains. Example: Alpe Arami (Central Swiss Alps). In: Basu, A., Hart, S.R. (Eds.), Earth Processes: Reading the Isotopic Code. American Geophysical Union, pp. 309-328.

Hartley, M.E., Thordarson, T., Fitton, J.G., EIMF., 2013. Oxygen isotopes in melt inclusions and glasses from the Askja volcanic system, North Iceland. Geochimica et Cosmochimica Acta **123**, 55-73.

Hattori, K., Muehlenbachs, K., 1982. Oxygen isotope ratios of the Icelandic crust. Journal of Geophysical Research **87**, 6559-6565.

He, Q., Zhang, S.-B., Zheng, Y.-F., 2016. High temperature glacial meltwater-rock reaction in the Neoproterozoic: Evidence from zircon in-situ oxygen isotopes in granitic gneiss from the Sulu orogen. Precambrian Research **284**, 1-13.

Hoefs, J., 2015. Stable Isotope Geochemistry. 7th edition. Springer-Verlag, Berlin. 389 p.

Kaneko, Y., Katayama, I., Yamamoto, H., Misawa, K., Ishikawa, M., Rehman, H.U., Kausar, A.B., Shiraishi, K., 2003. Timing of Himalayan ultrahigh-pressure metamorphism: sinking rate and subduction angle of the Indian continental crust beneath Asia. Journal of Metamorphic Geology **21**, 589-599.

Kawahata, H., Kusakabe, M., Kikuchi, Y., 1987. Strontium, oxygen, and hydrogen

isotope geochemistry of hydrothermally altered and weathered rocks in DSDP hole 504B, Costa Rica rift. Earth and Planetary Science Letters **85**, 343-355.

Kita, N.T., Ushikubo, T., Fu, B., Valley, J.W., 2009. High precision SIMS oxygen isotope analysis and the effect of sample topography. Chemical Geology **264**, 43-57.

Kitajima, K., Ushikubo, T., Kita, N.T., Maruyama, S., Valley, J.W., 2012. Relative retention of trace element and oxygen isotope ratios in zircon from Archean rhyolite, Panorama Formation, North Pole Dome, Pilbara Craton, Western Australia. Chemical Geology **332-333**, 102-115.

Le Fort, P., Debon, F., Sonet, J., 1980. The "Lesser Himalayan" cordierite granite belt. Typology and age of the pluton of Mansehra (Pakistan). Proceedings of International Committee on Geodynamics, Group 6 Meeting, Peshawar, November 23-29, p. 179.

Liati, A., Gebauer, D., 1999. Constraining the prograde and retrograde P–T–t path of Eocene HP rocks by SHRIMP dating different zircon domains: inferred rates of heating, burial, cooling and exhumation for central Rhodope, northern Greece. Contributions to Mineralogy and Petrology **135**, 340-354.

Liu, D., Ping Jian, P., Kröner, A., Xu, S., 2006. Dating of prograde metamorphic events deciphered from episodic zircon growth in rocks of the Dabie-Sulu UHP complex, China. Earth and Planetary Science Letters **250**, 650-666.

Miller, C. Thöni, M., Frank, W., Grasemann, B., Klötzli, U., Guntli, P., Dragantis, E., 2001. The early Paleozoic magmatic event in the Northwest Himalaya, India: source, tectonic setting and age of emplacement. Geological Magazine **138**, 237-251.

546 Naeem, M., Burg, J. P., Ahmad, N., Chaudhry, M. N., Khalid P., 2016. U-Pb zircon
547 systematic of the Mansehra Granitic Complex: implications on the early Paleozoic
548 orogenesis in NW Himalaya of Pakistan. Geosciences Journal **20**, 427-447.
549 O'Brien, P.J., Zotov, N., Law, R., Khan, M.A., Jan, M. Q., 2001. Coesite in Himalayan
550 eclogite and implications for models of India-Asia collision. Geology **29**, 435-438.
551 Page, F.Z., Ushikubo, T., Kita, N.T., Riciputi, L.R., Valley, J.W., 2007. High-precision
552 oxygen isotope analysis of picogram samples reveals 2μm gradients and slow
553 diffusion in zircon. American Mineralogist **92**, 1772-1775.
554 Peck, W.H., Valley, J.W., Graham, C.M., 2003. Slow oxygen diffusion rates in igneous
555 zircons from metamorphic rocks. American Mineralogist **88**, 1003-1014.
556 Polyakov, V. B., Kharlashina, N. N., 1994. Effect of pressure on equilibrium isotopic
557 fractionation, Geochimica et Cosmochimica Acta **58**, 4739-4750.
558 Quinn, R.J., Kitajima, K., Nakashima, D., Spicuzza, M.J., Valley, J.W., 2016. Oxygen
559 isotope thermometry using quartz inclusions in garnets. Journal of Metamorphic
560 Geology **35**, 231-252.
561 Rehman, H.U., Yamamoto, H., Kaneko, Y., Kausar, A.B., Murata, M., Ozawa, H., 2007.
562 Thermobaric structure of the Himalayan metamorphic belt in Kaghan Valley,
563 Pakistan. Journal of Asian Earth Sciences **29**, 390-406.
564 Rehman, H.U., Kobayashi, K., Tsujimori, T., Ota, T., Yamamoto, H., Nakamura, E.,
565 Kaneko, Y., Khan, T., Terabayashi, M., Yoshida, K., Hirajima, T., 2013a. Ion
566 microprobe U–Th–Pb geochronology and study of micro-inclusions in zircon from
567 the Himalayan high and ultrahigh-pressure eclogites, Kaghan Valley of Pakistan.
568 Journal of Asian Earth Sciences **63**, 179-196.
569 Rehman, H.U., Yamamoto, H., SHIN K., 2013b. Metamorphic P–T evolution of high-

570 pressure eclogites from garnet growth and reaction textures: Insights from the
571 Kaghan Valley transect, northern Pakistan. Island Arc **22**, 4-24.
572 Rehman, H.U., Tanaka, R., O'Brien, P.J., Kobayashi, K., Tsujimori, T., Nakamura, E.,
573 Yamamoto, H., Khan, T., Kaneko, Y., 2014. Oxygen isotopes in Indian Plate
574 eclogites (Kaghan Valley, Pakistan): Negative $\delta^{18}O$ values from a high latitude
575 protolith reset by Himalayan metamorphism. Lithos **208-209**. 471-483.
576 Rehman, H.U., Lee, H.Y., Chung, S.L., Khan, T., O'Brien, P.J., Yamamoto, H., 2016.
577 Source and mode of the Permian Panjal Trap magmatism: Evidence from zircon
578 U–Pb and Hf isotopes and trace element data from the Himalayan ultrahigh-
579 pressure rocks. Lithos **260**, 286-299.
580 Rehman, H.U., Jan, M.Q., Khan, T., Yamamoto, H., Kaneko, Y., 2017. Varieties of the
581 Himalayan eclogites: A pictorial review of textural and petrological features. Island
582 Arc **26**, 1-14 (e12209).
583 Rumble, D., Giorgis, D., Ireland, T., Zhang, Z., Xu, H., Yui, T. F., Yang, J., Xu, Z.,
584 2002. Low $\delta^{18}O$ zircons, U–Pb dating, and the age of the Qinglongshan oxygen
585 and hydrogen isotope anomaly near Donghai in Jiangsu Province, China.
586 Geochimica et Cosmochimica Acta **66**, 2299-2306.
587 Schulze, D.J., Harte, B., E.I.M.F., Page, F.Z., Valley, J.W., Channer, D.M.D.R., Jaques,
588 A.L., 2013. Anticorrelation of isotope signatures of carbon in eclogitic diamonds
589 and oxygen in their silicate mineral inclusions requires subducted source material
590 for eclogitic diamonds. Geology **41**, 455-458.
591 Valley, J.W., 1986. Stable isotope geochemistry of metamorphic rocks, in: Valley, J.W.,
592 Taylor, H.P. Jr., O'Neil, J.R. (Eds.), Stable Isotopes in High Temperature
593 Geological Processes, Reviews in Mineralogy **16**, 445-489.

Valley, J.W., Chiarenzelli, J.R., McLelland, J.M., 1994. Oxygen isotope chemistry of zircon. Earth and Planetary Science Letters **126**, 187-206.

Valley, J.W., Kinny, P.D., Schulze, D.J., Spicuzza, M.J., 1998. Zircon megacrysts from kimberlite: oxygen isotope variability among mantle melts. Contributions to Mineralogy and Petrology **133**, 1-11.

Valley, J.W., 2003. Oxygen isotopes in zircon. In: Hanchar, J.M., Hoskin, W.O. (Eds.), Reviews in Mineralogy and Geochemistry **53**, 343-385.

Valley, J.W., Bindeman, I.N., Peck, W.H., 2003. Empirical calibration of oxygen isotope fractionation in zircon. Geochimica et Cosmochimica Acta **67**, 3257-3266.

Valley, J.W., Lackey, J.S., Cavosie, A.J., Clechenko, C.C., Spicuzza, M.J., Basei, M.A.S., Bindeman, I.N., Ferreira, V.P., Sial, A.N., King, E.M., Peck, W.H., Sinha, A.K., Wei, C.S., 2005. 4.4 billion years of crustal maturation: oxygen isotope ratios of magmatic zircon. Contributions to Mineralogy and Petrology **150**, 561-580.

Valley, J.W., Kita, N.T., 2009. In situ oxygen isotope geochemistry by ion microprobe. Mineralogical Association of Canada Short Course **41**, 19-63.

Valley, J.W., Reinhard, D.A., Cavosie, A.J., Ushikubo, T., Lawrence, D.F., Larson, D.J., Kelly, T.F., Snoeyenbos, D., Strickland, A., 2015. Nano- and Micro-geochronology in Hadean and Archean Zircons by Atom-Probe Tomography and SIMS: New Tools for Old Minerals. American Mineralogist, **100**, 1355-1377. doi.org/10.2138/am-2014-5134.

Wan, Y.S., Zhang, J.H., Williams, I.S., Liu, D.Y., Dong, C.Y., Fan, R.L., Shi, Y.R., Ma, M.Z., 2013. Extreme zircon O isotopic compositions from 3.8 to 2.5 Ga magmatic rocks from the Anshan area, North China Craton. Chemical Geology **352**, 108-124.

Wang, X.C., Li, Z. X., Li, X. H., Li, Q.L., Tang, G.Q., Zhang, Q.R., Liu, Y., 2011.

618 Nonglacial origin for low-$\delta^{18}O$ Neoproterozoic magmas in the South China Block:
619 evidence from new in-situ oxygen isotope analysis using SIMS. Geology **39**, 735-
620 738.
621 Wang, X.-L., Coble, M.A., Valley, J.W., Shu, X.-J., Kitajima, K., Spicuzza, M.J., Sun, T.,
622 2014. Influence of radiation damage on late Jurassic zircon from southern China:
623 Evidence from in situ measurement of oxygen isotopes, laser Raman, U-Pb ages,
624 and trace elements. Chemical Geology, **389**, 122-136.
625 Wasserburg, G.J., Papanastassiou, D.A., Nenow, E.V., Baumann, C.A., 1969. A
626 programmable magnetic field mass spectrometer with on-line data processing.
627 Reviews of Scientific Instruments **40**, 288-295.
628 Watson, E.B., Cherniak, D.J., 1997. Oxygen diffusion in zircon. Earth Planetary Science
629 Letters **148**, 527-544.
630 Wei, C.S., Zheng, Y.F., Zhao, Z.F., Valley, J.W., 2002. Oxygen and neodymium
631 isotope evidence for recycling of juvenile crust in northeast China. Geology **30**,
632 375-378.
633 Wei, C. S., Zhao, Z. F., Spicuzza, M. J., 2008. Zircon oxygen isotopic constraint on the
634 sources of late Mesozoic A-type granites in eastern China. Chemical Geology **250**,
635 1-15.
636 Yui, T.F., Rumble, D., Lo, C.H., 1995. Unusually low $\delta^{18}O$ ultra-high-pressure
637 metamorphic rocks from the Sulu Terrain, eastern China. Geochimica et
638 Cosmochimica Acta **59**, 2859-2864.
639 Zhao, Z.F., Zheng, Y.F., 2003. Calculation of oxygen isotope fractionation in magmatic
640 rocks. Chemical Geology **193**, 59-80.
641 Zheng, Y.F., Fu, B., Li, Y., Xiao, Y., Li, S., 1998. Oxygen and hydrogen isotope

642 geochemistry of ultrahigh-pressure eclogites from the Dabie Mountains and the
643 Sulu terrane. Earth Planetary Science Letters **155**, 113-129.
644 Zheng, Y.F., Fu, B., 1998. Estimation of oxygen diffusivity from anion porosity in
645 minerals. Geochemical Journal **32**, 71-89.
646 Zheng, Y.F., Fu, B., Gong, B. and Li, L., 2003. Stable isotope geochemistry of ultrahigh
647 pressure metamorphic rocks from the Dabie-Sulu orogen in China: implications for
648 geodynamics and fluid regime. Earth Science Review **62**, 105-161.
649 Zheng, Y. F., Wu, Y.-B., Chen, F.K., Gong, B., Li, L., Zhao, Z.F., 2004. Zircon U-Pb
650 and oxygen isotope evidence for a large-scale ^{18}O depletion event in igneous rocks
651 during the Neoproterozoic. Geochimica et Cosmochimica Acta **68**, 4145-4165.
652 Zheng, Y. F., Wu, Y.-B., Gong, B., Chen, R.-X., Tang, J., Zhao, Z. F., 2007. Tectonic
653 driving of Neoproterozoic glaciations: Evidence from extreme oxygen isotope
654 signature of meteoric water in granite. Earth and Planetary Science Letters **256**,
655 196-210.
656 Zheng, Y. F., Gong, B., Zhao, Z. F., Wu, Y.B., Chen, F.K., 2008. Zircon U-Pb age and
657 O isotope evidence for Neoproterozoic low-^{18}O magmatism during
658 supercontinental rifting in South China: implications for snowball Earth event.
659 American Journal of Sciences **308**, 484-516.
660 Zhu, D.C., Zhao, Z.D., Niu, Y., Dilek, Y., Wang, Q., Ji, W.H., Dong, G.C., Sui, Q.L.,
661 Liu, Y.S., Yuan, H.L., Mo, X.X., 2012. Cambrian bimodal volcanism in the Lhasa
662 Terrane, southern Tibet: Record of an early Paleozoic Andean-type magmatic arc
663 in the Australian proto-Tethyan margin. Chemical Geology **328**, 290-308.

664 **Captions of Figures and Tables**

665

666 **Fig. 1.** Geological map of the study area (a) regional geological sketch, (b) major
667 tectonic units of the western Himalaya, (c) geological cross-section along the Kaghan
668 Valley transect with sample location, and (d) an enlarged view of a portion where the
669 samples were collected.

670 **Fig. 2.** SEM-cathodoluminescence images of the analyzed zircons from Group I
671 eclogites. Numbers in the circles with a, b, c suffixes are the zircon numbers (to see
672 them in table S1). The same grains were analyzed for LA-ICP-MS U–Pb and Hf isotope
673 ratios. In situ SIMS $\delta^{18}O$ analyses are also shown. Zircons from mount Ph380_Zrn3
674 were picked from same sample (Ph380) and were analyzed for $\delta^{18}O$ values only. We
675 assume those grains have identical age and Hf isotope composition. Scale bar shown for
676 each grain is 50 μm.

677 **Fig. 3.** SEM-cathodoluminescence images of the analyzed zircons from Group II
678 eclogites. Other details are the same as in Fig. 2; disc. = discordant in age.

679 **Fig. 4.** SEM-cathodoluminescence images of the analyzed zircons from felsic gneisses.
680 Other details are the same as in Fig. 2.

681 **Fig. 5.** SIMS $\delta^{18}O$ values in zircon plotted against U–Pb age (Ma).

682 **Fig. 6.** Values of $\delta^{18}O$ in zircons (dark thick line) and whole rock (boxes) from eclogites
683 and gneisses of the Kaghan Valley. Data for other rock types and for zircons of different
684 origins are also shown for comparison (data adopted from Valley et al., 2005).

685 **Fig. 7.** Values of $\delta^{18}O$ for zircons and whole-rock (WR) plotted against εHf (t). Data for
686 zircons of different origin are shown for comparison (data for $\delta^{18}O$ adopted from Valley
687 et al., 2005 and Valley and Kita, 2009). Symbols used are same as in Fig. 5. Values for
688 $\delta^{18}O$ of seawater and meteoric water are arbitrarily plotted along the Y-axis and do not
689 imply a value of [εHf(t)].

690 **Fig. 8.** Values of $\delta^{18}O$ plotted against background-corrected ratios of $^{16}O^{1}H/^{16}O$
691 (supplementary table S1). The concentration of water and OH is negligible in these
692 zircons and there is no correlation with $\delta^{18}O$, indicating an absence of secondary effects
693 or radiation damage.

694 **Fig. 9.** Values of $\delta^{18}O$ for zircon (averaged for all the analyzed spots) plotted against
695 averaged values of quartz and garnet for the samples from same group. The
696 equilibration lines are drawn as $\delta^{18}O_{quartz\text{-}zircon} = 2‰$, and $\delta^{18}O_{garnet\text{-}zircon} = 0‰$. 2SD error
697 bars are not shown as they are smaller than the symbol size plotted on the figure.

698

699 **Table 1.** Oxygen isotope data for the zircon from the Himalayan UHP rocks measured
700 by CAMECA IMS 1280 at WiscSIMS.

701 Foot note to Table 1: The precision of individual analyses was estimated by two
702 standard deviations (2SD) of the reproducibility of bracketing standard analyses.

703

704 **Supplementary table S1.** In situ SIMS oxygen isotope data from the analyzed zircons.

705

706 Foot note to S1: During analysis the actual primary intensity "IP (nA)" was kept
707 between 0.15-6nA, higher than the values given in the table. Analysis #62, 78, and 79 of
708 the standard (values strikethrough) are excluded from calculating the average values
709 (probably affected by some hidden crack or inclusion etc.).

710

711 **Supplementary table S2.** Values of $\delta^{18}O$ (in ‰ relative to VSMOW) of whole rock
712 (WR) and constituent minerals. Values of $\delta^{18}O$ were measured using the laser
713 fluorination technique (data reproduced from Rehman et al., 2014).

Highlights

- Zircons in the Himalayan ultrahigh-pressure eclogites were formed from a subducted low-$\delta^{18}O$ (hydrothermally altered) oceanic crustal source.
- The protoliths of the Himalayan eclogites were further hydrothermally altered by high-temperature meteoric-water interaction before eclogite facies metamorphism.
- During the Himalayan ultrahigh-pressure metamorphism new low-$\delta^{18}O$ minerals crystallized from the $\delta^{18}O$-depleted precursors.

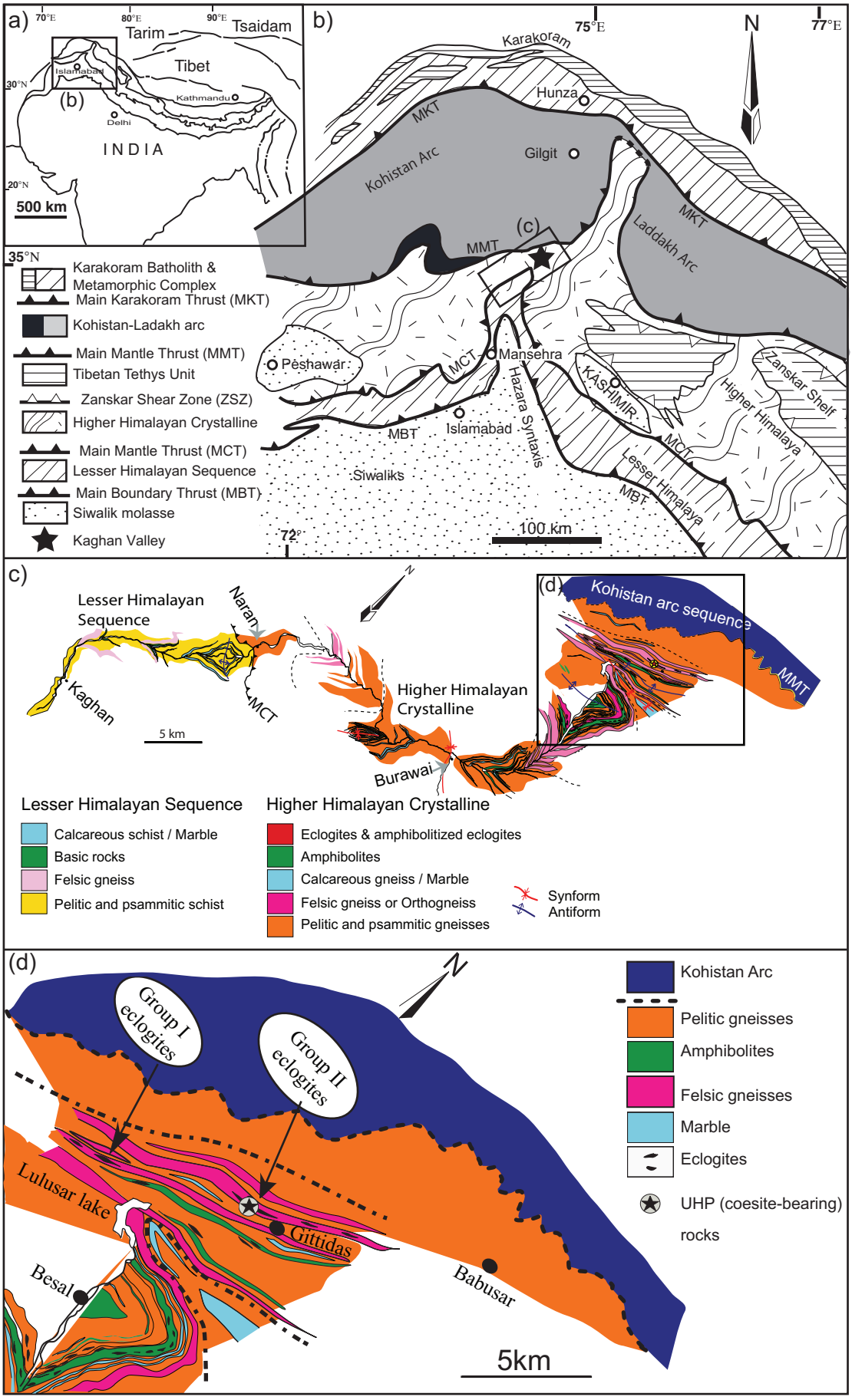

Fig. 1. (Rehman et al.)

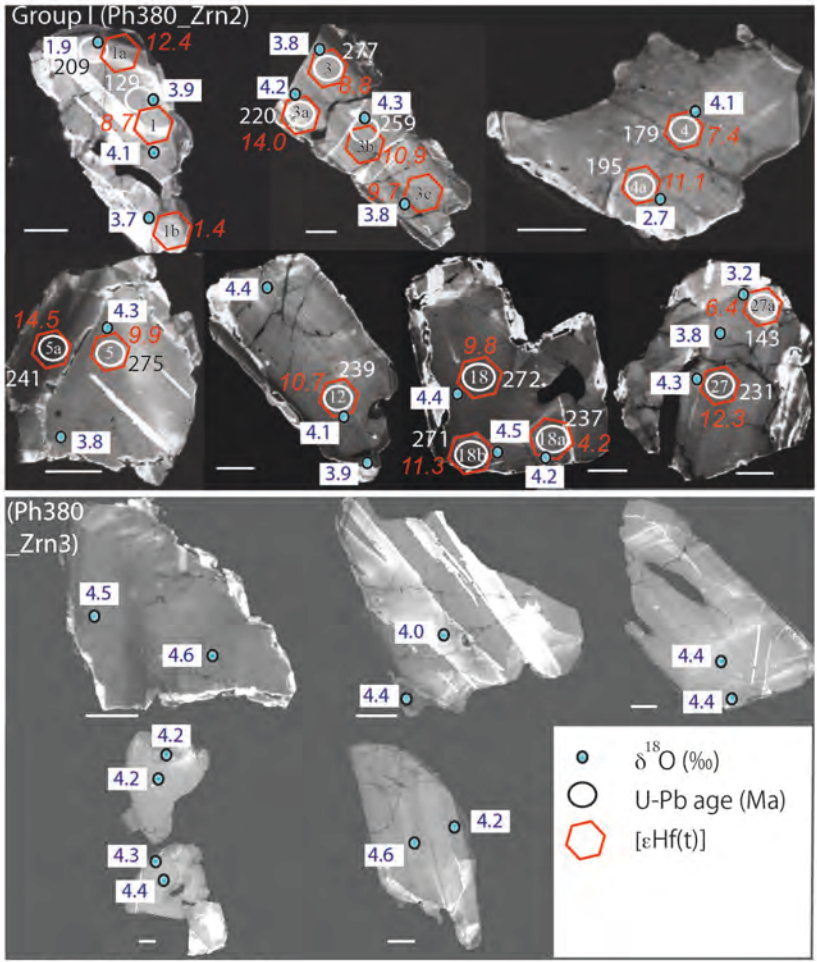

Fig. 2. (Rehman et al.)

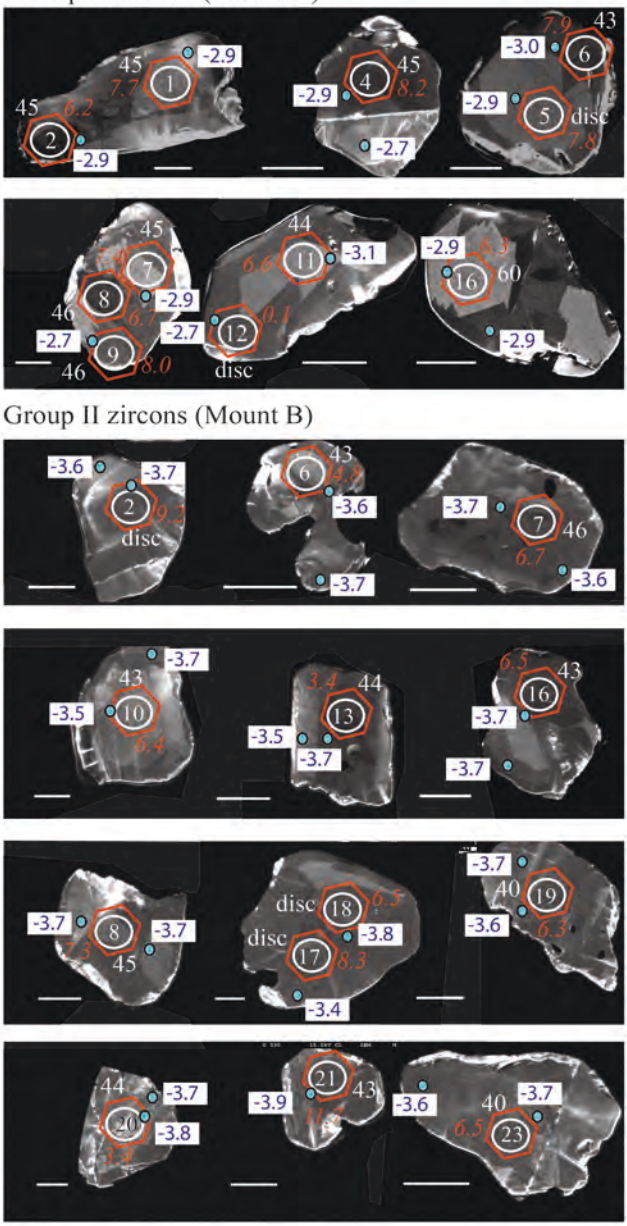

Fig. 3. (Rehman et al.)

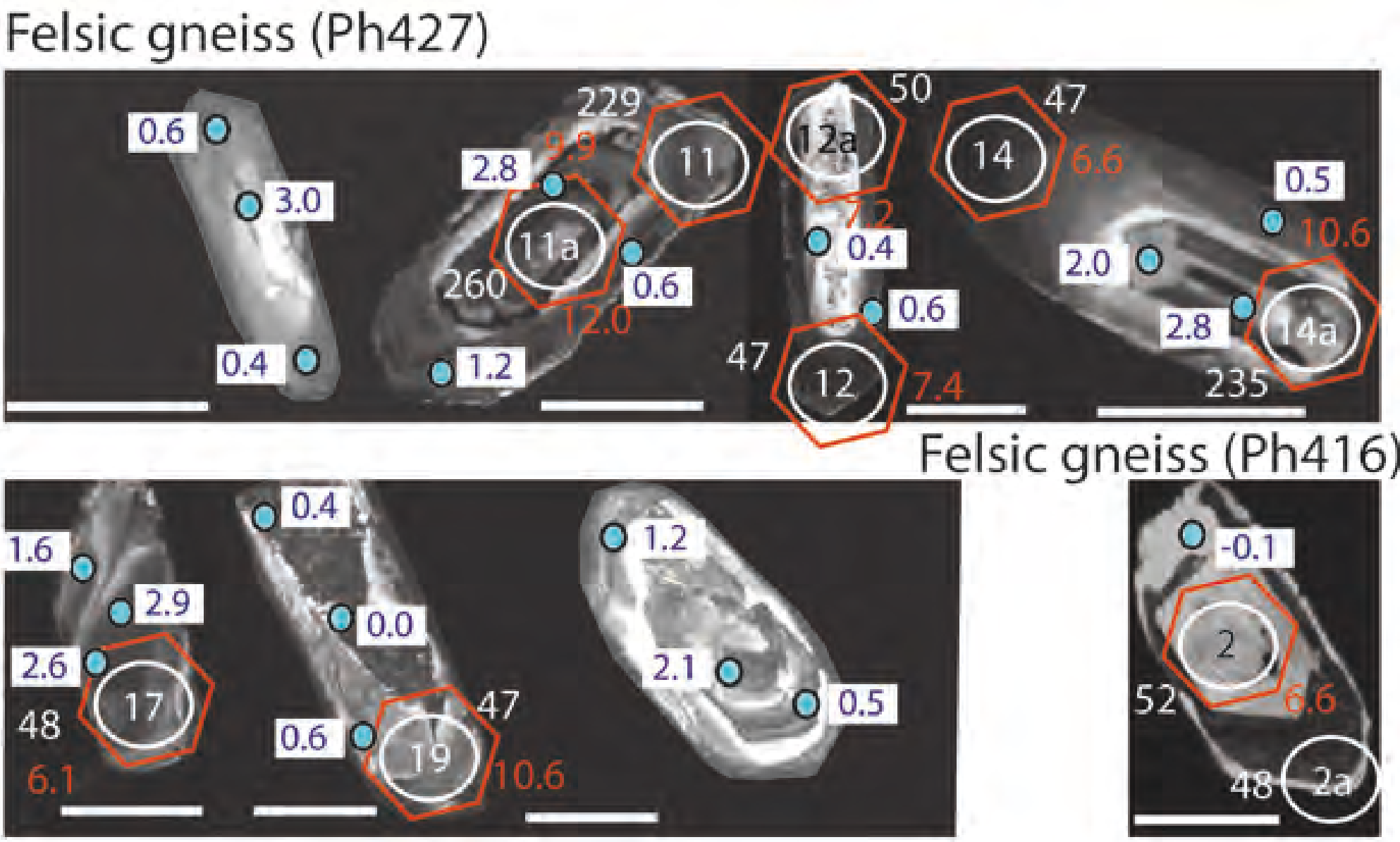

Fig. 4. (Rehman et al.)

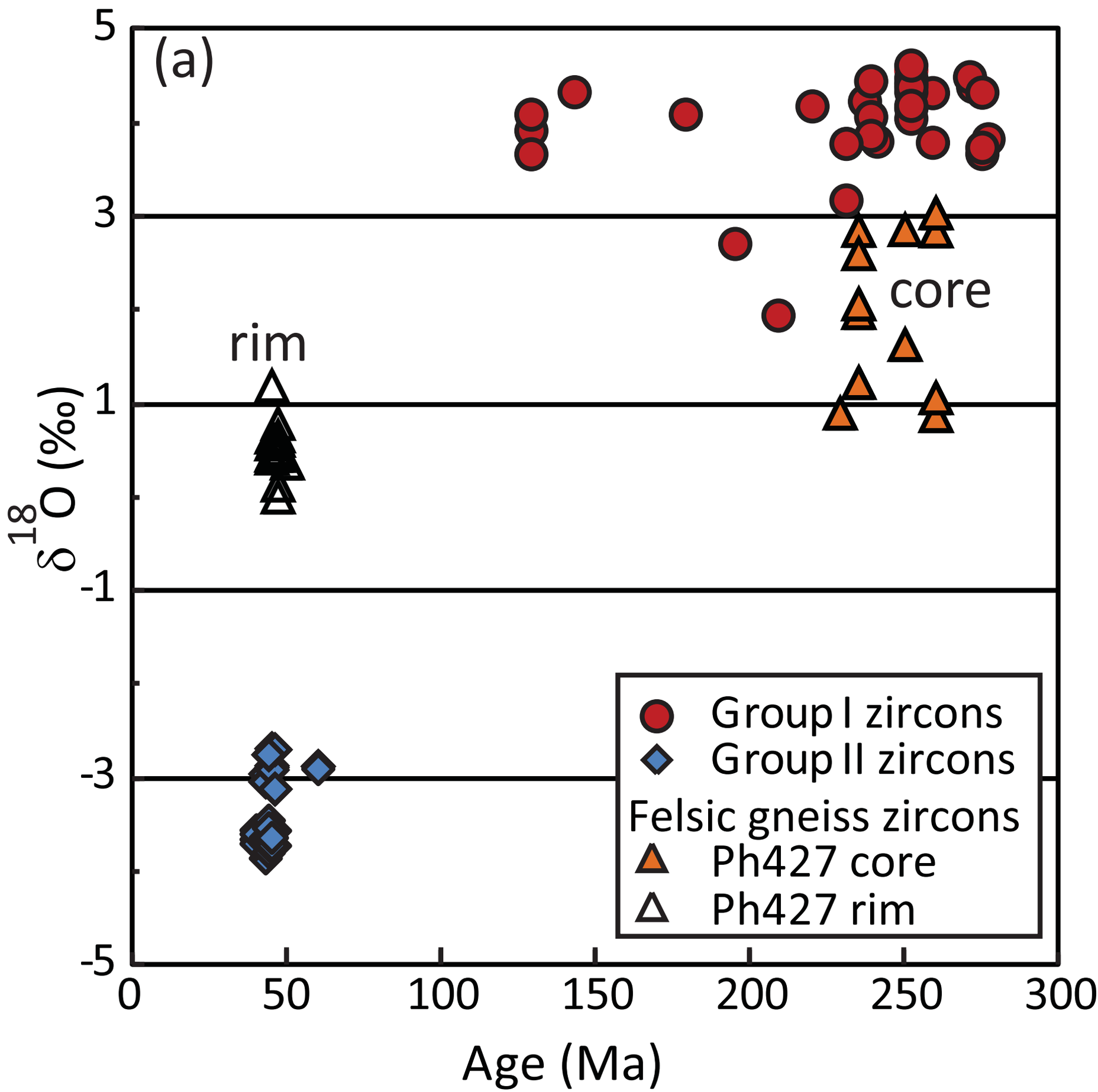

Fig. 5. (Rehman et al.)

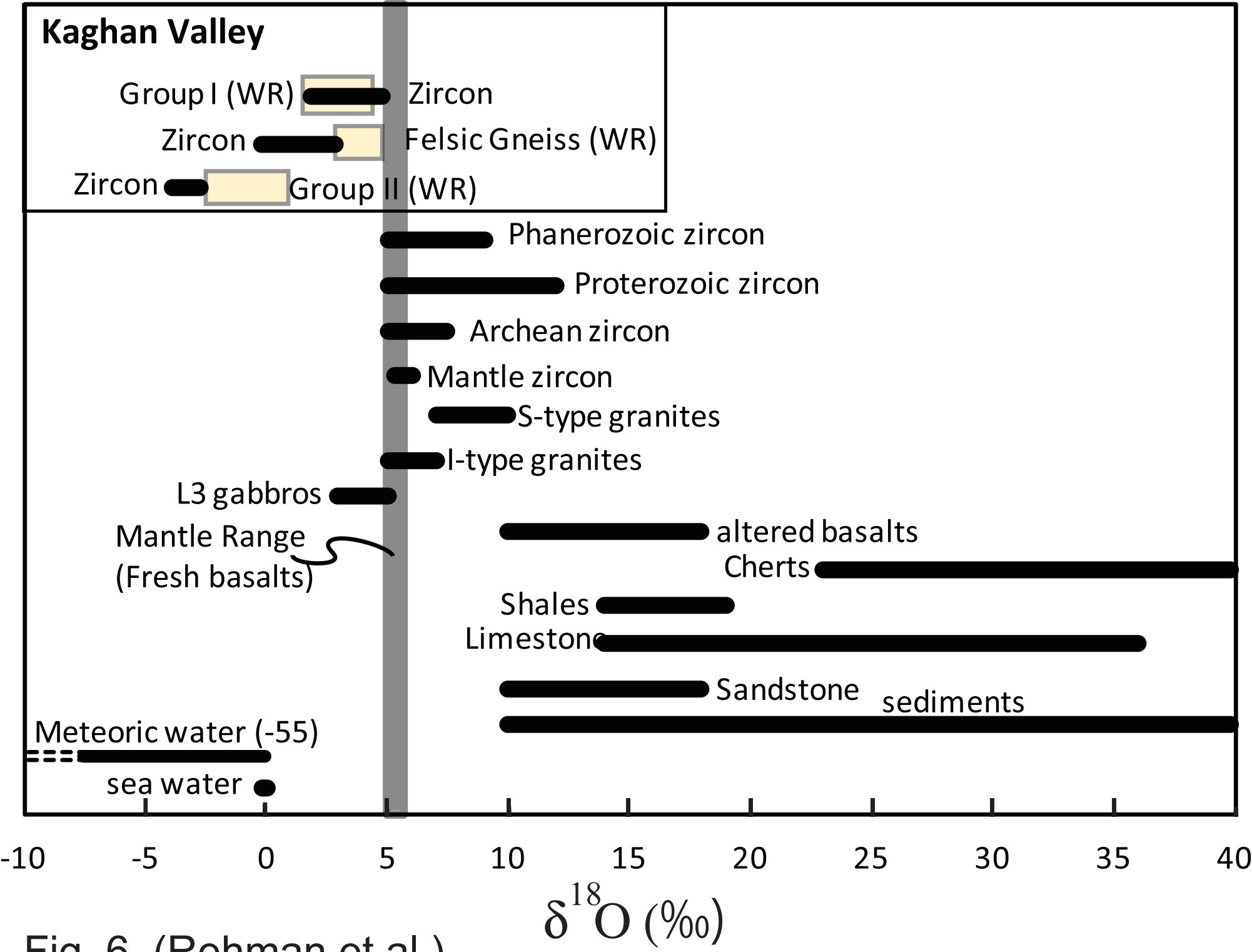

Fig. 6. (Rehman et al.)

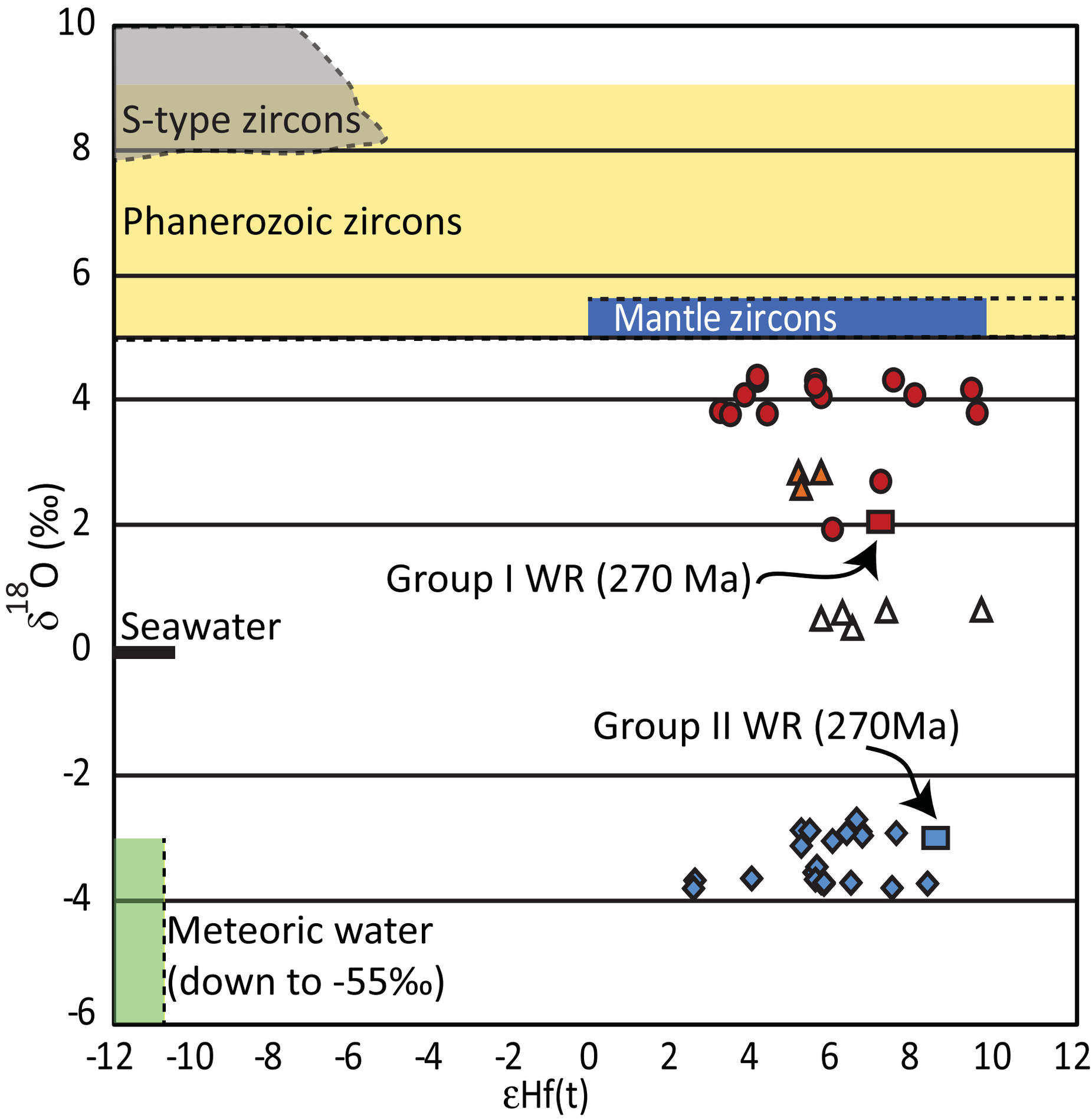

Fig. 7. (Rehman et al.)

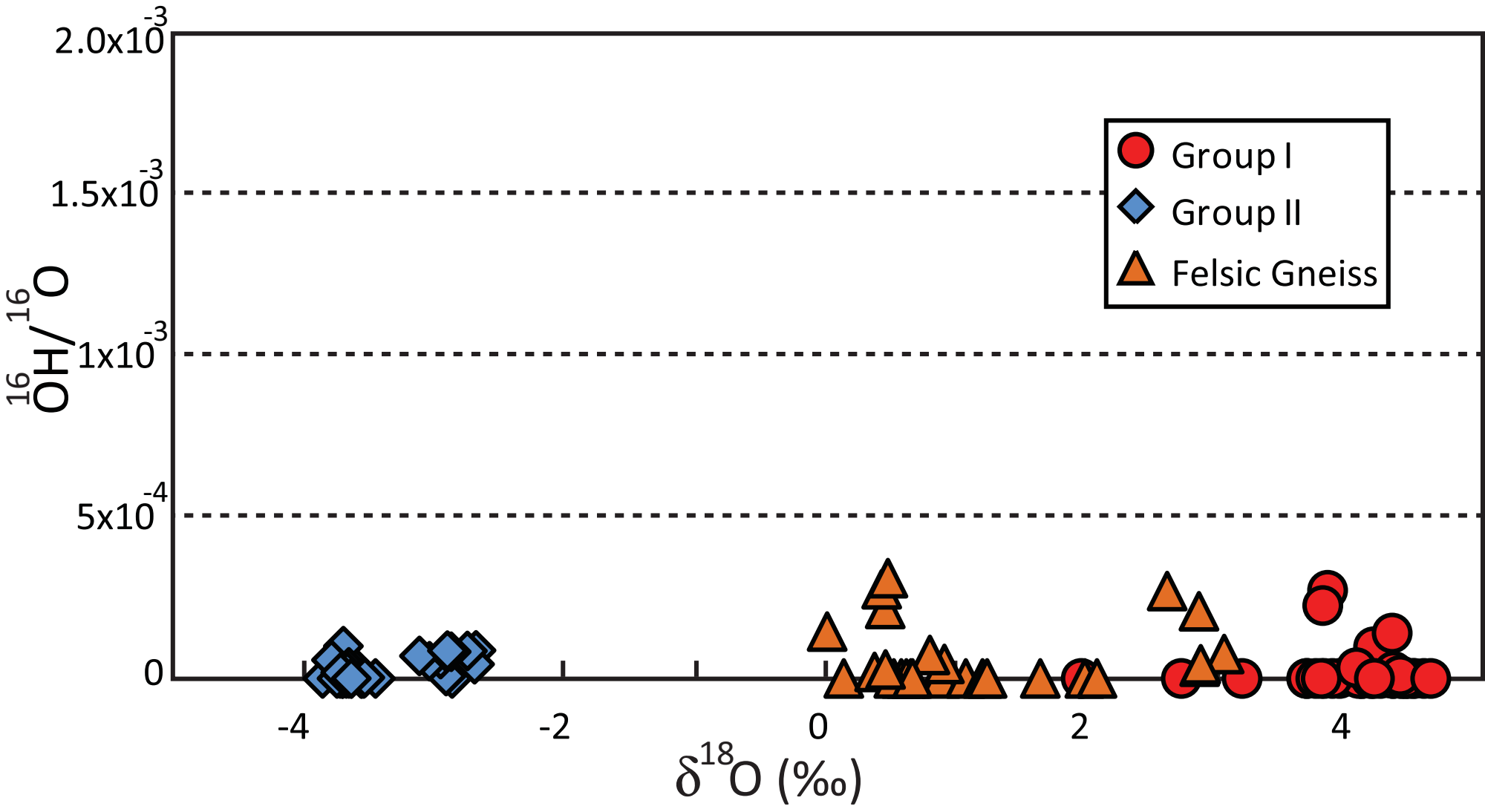

Fig. 8. (Rehman et al.)

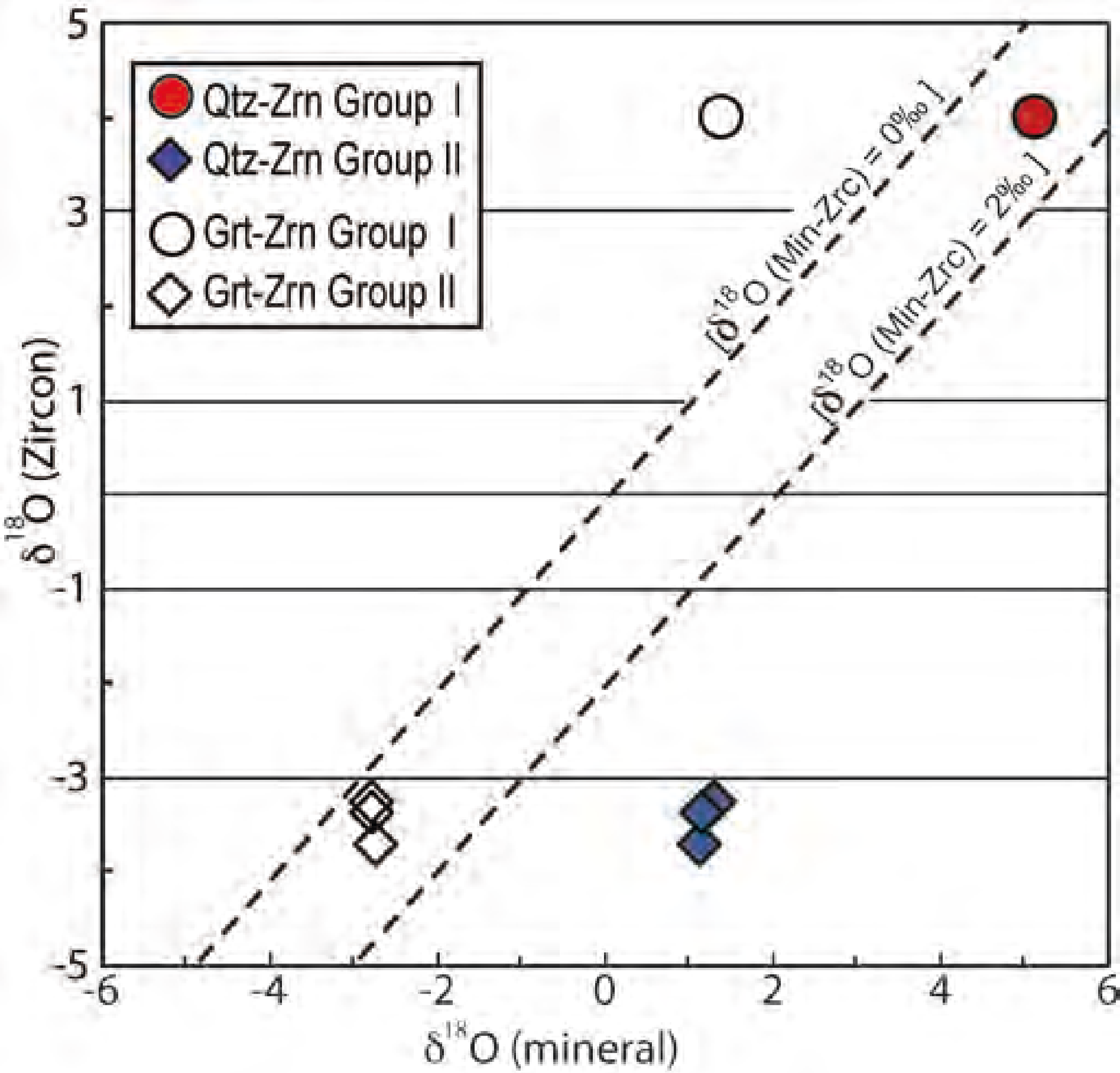

Fig. 9. (Rehman et al.)

Table 1. Oxygen isotope data for the zircon from the Himalayan UHP rocks measured by CAMECA IMS 1280 at WiscSIMS.

Analysis#	Sample	δ18O ‰ VSMOW	2SD (ext.)	δ18O ‰ measured	2SE (int.)		Analysis#	Sample	δ18O ‰ VSMOW	2SD (ext.)	δ18O ‰ measured	2SE (int.)
Group I							**Group II (Mount B)**					
(Ph380_Zrn2)							28	422_Zrn01_1	-3.66	0.27	-2.23	0.23
88	Zrn18_1	4.39	0.23	4.73	0.20		29	422_Zrn01_2	-3.56	0.27	-2.13	0.23
89	Zrn18_2	4.49	0.23	4.84	0.21		30	422_Zrn02_1	-3.80	0.27	-2.37	0.15
90	Zrn18_3	4.23	0.23	4.58	0.23		31	422_Zrn02_2	-3.68	0.27	-2.26	0.14
91	Zrn01_1	1.95	0.23	2.29	0.16		32	422_Zrn05_1	-3.86	0.27	-2.43	0.20
92	Zrn01_2	3.92	0.23	4.26	0.16		33	422_Zrn07_1	-3.70	0.27	-2.27	0.21
93	Zrn01_3	4.09	0.23	4.44	0.21		34	422_Zrn07_2	-3.60	0.27	-2.17	0.21
94	Zrn01_4	3.67	0.23	4.01	0.20		35	423_Zrn18_1	-3.70	0.27	-2.27	0.18
95	Zrn03_1	3.83	0.23	4.17	0.22		36	423_Zrn18_2	-3.66	0.27	-2.23	0.19
96	Zrn03_2	4.18	0.23	4.52	0.22		37	423_Zrn23_1	-3.79	0.27	-2.36	0.32
97	Zrn03_3	4.32	0.23	4.67	0.26		38	423_Zrn23_2	-3.45	0.27	-2.03	0.21
98	Zrn03_4	3.79	0.23	4.13	0.23		44	425_Zrn03_1	-3.64	0.29	-2.17	0.20
103	Zrn04_1	4.09	0.22	4.31	0.17		45	425_Zrn03_2	-3.68	0.29	-2.21	0.19
104	Zrn04_2	2.71	0.22	2.93	0.17		46	425_Zrn04_1	-3.72	0.29	-2.26	0.20
105	Zrn05_1	4.33	0.22	4.54	0.22		47	425_Zrn04_2	-3.56	0.29	-2.09	0.22
106	Zrn05_2	3.81	0.22	4.02	0.20		48	425_Zrn05_1	-3.71	0.29	-2.24	0.24
107	Zrn08_1	3.67	0.22	3.89	0.14		49	425_Zrn05_2	-3.71	0.29	-2.24	0.18
108	Zrn08_2	3.74	0.22	3.95	0.24		50	425_Zrn07_1	-3.54	0.29	-2.07	0.21
109	Zrn12_1	4.07	0.22	4.28	0.24		51	425_Zrn07_2	-3.75	0.29	-2.28	0.23
110	Zrn12_2	3.87	0.22	4.08	0.24		52	425_Zrn11_1	-3.67	0.29	-2.20	0.22
111	Zrn12_3	4.45	0.22	4.66	0.20		53	425_Zrn11_2	-3.53	0.29	-2.07	0.24
112	Zrn24_1	4.57	0.22	4.78	0.17		54	425_Zrn17_1	-3.72	0.29	-2.25	0.22
113	Zrn24_2	4.48	0.22	4.70	0.25		55	425_Zrn17_2	-3.64	0.29	-2.17	0.20
114	Zrn27_1	3.18	0.22	3.39	0.15			**Average**	**-3.40**			
115	Zrn27_2	3.78	0.22	4.00	0.23			**Average 2SD**		**0.40**		
116	Zrn27_3	4.33	0.22	4.55	0.21		**Felsic gneiss (Ph427)**					
Group I							125	Zrn3_1	0.87	0.09	1.29	0.30
(Ph380_Zrn3)							126	Zrn3_2	1.06	0.09	1.49	0.17
169	Zrn20_1	4.43	0.22	4.64	0.18		127	Zrn3_3	0.90	0.09	1.32	0.23
170	Zrn20_2	4.40	0.22	4.61	0.22		128	Zrn4_1	0.13	0.09	0.55	0.19
171	Zrn21_1	4.16	0.22	4.37	0.19		129	Zrn4_2	0.45	0.09	0.87	0.26
172	Zrn21_2	4.17	0.22	4.38	0.20		130	Zrn4_3	0.79	0.09	1.21	0.21
173	Zrn22_1	4.43	0.22	4.64	0.19		131	Zrn11_1	2.85	0.09	3.27	0.19
174	Zrn22_2	4.34	0.22	4.55	0.24		132	Zrn11_2	0.64	0.09	1.06	0.22
175	Zrn19_1	4.05	0.22	4.26	0.17		133	Zrn11_3	1.19	0.09	1.61	0.20
176	Zrn19_2	4.39	0.22	4.60	0.24		134	Zrn10_1	3.04	0.09	3.46	0.14
177	Zrn23_1	4.62	0.22	4.83	0.24		135	Zrn10_2	0.57	0.09	0.99	0.23
178	Zrn23_2	4.19	0.22	4.40	0.21		136	Zrn10_3	0.42	0.09	0.84	0.23
	Average	**4.03**		4.28	0.21		141	Zrn12_1	0.36	0.12	0.77	0.21
	Average 2SD		**0.22**				142	Zrn12_2	0.61	0.12	1.01	0.17
Group II							143	Zrn14_1	2.85	0.12	3.26	0.23
(Mount A)							144	Zrn14_2	0.51	0.12	0.92	0.21
66	423_Zrn07_1	-2.89	0.63	-2.21	0.17		145	Zrn14_3	1.97	0.12	2.38	0.22
67	423_Zrn07_2	-2.87	0.63	-2.19	0.21		146	Zrn17_1	2.60	0.12	3.01	0.20
68	423_Zrn15_1	-2.91	0.63	-2.24	0.16		147	Zrn17_2	1.63	0.12	2.04	0.19
69	423_Zrn15_2	-2.68	0.63	-2.01	0.16		148	Zrn17_3	2.86	0.12	3.27	0.18
70	425_Zrn02_1	-2.95	0.63	-2.28	0.17		149	Zrn19_1	0.65	0.12	1.06	0.22
71	425_Zrn02_2	-3.04	0.63	-2.37	0.19		150	Zrn19_2	0.00	0.12	0.41	0.25
72	425_Zrn03_1	-2.91	0.63	-2.24	0.22		151	Zrn20_1	2.07	0.12	2.47	0.14
73	425_Zrn03_2	-2.69	0.63	-2.02	0.19		152	Zrn20_2	0.47	0.12	0.87	0.19
74	425_Zrn06_1	-3.12	0.63	-2.44	0.32		153	Zrn20_3	1.23	0.12	1.63	0.17
75	425_Zrn06_2	-2.75	0.63	-2.08	0.18		154	Zrn19_3	0.45	0.12	0.85	0.17
76	425_Zrn18_1	-2.87	0.63	-2.20	0.22		**Felsic gneiss (Ph416A)**					
77	425_Zrn18_2	-2.90	0.63	-2.23	0.23		164	Zrn2_1	-0.09	0.11	0.21	0.21